Spectroscopic Probes of the Quasi-Liquid Layer on Ice

T. F. Kahan,[†] J. P. Reid,[‡] and D. J. Donaldson*,[†]

Department of Chemistry, University of Toronto, 80 Saint George Street, Toronto, Ontario, Canada M5S 3H6, School of Chemistry, University of Bristol, Bristol, U.K. BS8 1TS

Raman spectra of the water OH-stretch region were acquired at air−ice and air−water interfaces at a glancing angle, which allowed observation of surface characteristics. The shapes of the OH-stretch bands indicate that the environment at the air−ice interface is different from that at the air−water interface and from that seen in bulk water. Water spectra measured at the surface of dodecane under low relative humidity indicate that this method is sensitive to fewer than 50 monolayers of water. Changes in the local environment of the surfacial water molecules may be induced by the presence of different solute species, giving rise to changes in the shape of the band. Dissolved sodium chloride disrupts hydrogen bonding in liquid water and has the same effect at the air−ice interface. However, when either HCl or HNO_3 is adsorbed from the gas phase onto an ice surface, the opposite effect is seen: Their presence appears to increase the extent of hydrogen bonding at the ice surface. At the same time, shifts in the laser-induced fluorescence spectra of acridine, a fluorescent pH-probe present at the air−ice interface, indicate that dissociation of acids occurs there. These observations suggest that the formation of hydronium ions at the air−ice interface enhances the hydrogen bonding of surfacial water molecules.

Introduction

The interface between ice and air has been the object of study for over a century. At temperatures not too far below water's freezing point, such as those encountered at Earth's surface, the highly ordered ice matrix gives way to a more disordered region near the air−ice interface, which is often referred to as the quasi-liquid layer (QLL). Some recent studies of physical properties of the QLL are discussed in refs 1−8, and a review is given in ref 9. The QLL is important to the fate of atmospheric species that come in contact with ice: Deposition of a gas-phase species onto an ice surface will by necessity involve sorption onto or dissolution into the QLL. As well, contaminants such as salts can be excluded from the ice matrix during freezing, resulting in an enhancement of their concentrations in the QLL. This concentration enhancement is known to increase bimolecular reaction rates of a variety of compounds over those observed in the liquid phase (for example, see refs 10 and 11).

Recent experimental studies indicate that the photolysis rates of some organic species are enhanced in ice.[12,13] Work from this laboratory showed that photolysis of the aromatic compounds naphthalene and anthracene occurs in the QLL and that the rates are enhanced by up to a factor of 10 compared to the corresponding rates at a liquid water surface.[12] This rate enhancement, which has not yet been observed on other solid surfaces, is likely a consequence of the unique physical properties of the QLL. Further evidence of the different environment presented by the QLL is shown by the fluorescence spectra of naphthalene and anthracene which have adsorbed to the surface from the gas phase. On a water surface, deposition of these compounds results in fluorescence spectra that are

consistent with emission from monomers; however, on ice the fluorescence spectra of both species indicate significant self-association, even after very short deposition times.[12]

The idea that the QLL presents an environment that is different both from bulk ice and from liquid water is not new. Theoretical and experimental studies have long suggested that the physical properties of the QLL are distinct from those of solid and liquid water.[3,5,8] Measurements of the physical properties of the QLL are difficult, however, as its depth likely does not exceed 100 nm even at high temperatures[1,2,5,6] and its structure almost certainly is not uniform at all depths. Therefore, different measurement techniques, which are sensitive to varying levels of disorder in the ice matrix and to different depths of the QLL, have reported quite different values of QLL depth, density, and orientational order.[1−8]

The work reported here presents two novel spectroscopic probes for the QLL. The first uses glancing-angle Raman spectroscopy to study the extent of hydrogen bonding in the QLL via the shape of the water OH-stretching band. The second method uses glancing-angle laser-induced fluorescence (LIF) to probe acridine, a pH-sensitive fluorescent molecule, and thereby infer changes in pH occurring in the QLL. These complementary techniques enable us to observe the dissociation of acids and bases on the ice surface and to observe the effects of this dissociation on the structure of the QLL.

Experimental Section

1. Apparatus. The ice reaction chamber used for this study has been described in detail elsewhere.[12] Briefly, it consists of a ~500 mL Teflon box with side ports through which gases can be introduced and vented. A copper plate on the chamber floor is soldered to copper tubing, through which cooling fluid is circulated. The temperature of the plate is monitored using a thermistor attached to its surface; good thermal contact is assured

* To whom correspondence should be addressed. E-mail: jdonalds@chem.utoronto.ca.
† University of Toronto.
‡ University of Bristol.

Probes of the Quasi-Liquid Layer on Ice

J. Phys. Chem. A, Vol. 111, No. 43, 2007 **11007**

by using thermal grease. Experiments were carried out at temperatures ranging from −16 to 24 °C.

Raman scattering was induced by the unfocused 355 nm output of a frequency-tripled Nd:YAG laser (pulse energy ∼0.5 mJ), and acridine fluorescence was excited by the 337 nm output of a nitrogen laser (pulse energy ∼ 0.25 mJ). Each laser operated at a repetition rate of 10 Hz. The laser beam entered and exited the Teflon chamber through quartz windows and impinged on the surface of the sample at a glancing angle (>85° from the surface normal for Raman experiments and >80° from the surface normal for LIF experiments). The polarization of the input radiation was perpendicular to the surface normal for all LIF experiments. For the Raman experiments the input polarization was varied using a polarization rotator. At an incident angle of 87° from the surface normal, 67% of p-polarized (polarized in the plane of incidence) and 80% of s-polarized (polarized perpendicular to the plane of incidence) input radiation will be reflected at the air−ice interface.

Raman scattering and acridine fluorescence were collected perpendicular to the surface using a 7 mm diameter liquid light guide suspended 1 cm above the sample. After passing through a long-pass optical filter having 10% transmission at 370 nm, the Raman scattered radiation was imaged into a monochromator, and the transmitted intensity was detected by a photomultiplier tube and sent to a digital oscilloscope and computer for analysis. No optical filters were used in the LIF experiments. The digital oscilloscope averaged the intensity vs time signal over 64 laser shots, and then the data were sampled and stored by the computer. Spectra were obtained by manually scanning the monochromator in steps to give approximately 30 cm^{-1} separation between collected data points over the spectral range of interest.

At the liquid water surface, spectra were measured in the same reaction chamber but with the water sample contained in a Petrie dish. Raman scattered light was collected from above, as in the ice experiments. Bulk water Raman spectra were measured with the sample in a 1 cm × 1 cm quartz cuvette. The laser beam entered through the side of the cuvette, and the detected light was collected at 90° to the laser input in the horizontal plane. These experiments were all performed at room temperature.

2. Sample Preparation. Ice samples were prepared by freezing ∼0.5 mL water on a copper plate placed on the chamber floor. After freezing, the copper plate was briefly removed from the chamber to invert the ice samples by hand to present a flat surface to the laser. The surface area of the ice exposed to the air was ∼3 cm^2, and the ice thickness ∼1.5 mm. We assume always that the thermistor provides an accurate indication of the sample temperature. During the preparation of D_2O ice, steps were taken to reduce contamination by ambient H_2O: The copper plate used as a substrate was soaked in D_2O for several minutes before being placed in the chamber, and the chamber was purged with dry N_2 prior to depositing the liquid D_2O.

Deposition of gas-phase H_2O onto the D_2O ice surface was accomplished by flowing N_2 at a rate of 1 SLM through a flask containing liquid H_2O heated to ∼75 °C before introducing it to the chamber through the side port via ∼0.5 m of Tygon tubing at room temperature. Ice samples containing acridine were prepared by freezing ∼0.5 mL of a concentrated aqueous solution of acridine in the same manner as described above for pure water. Gas-phase HCl, HNO_3, and NH_3 were deposited on the ice surface by withdrawing ∼2 mL of the vapor present in the headspace of a bottle containing a concentrated aqueous
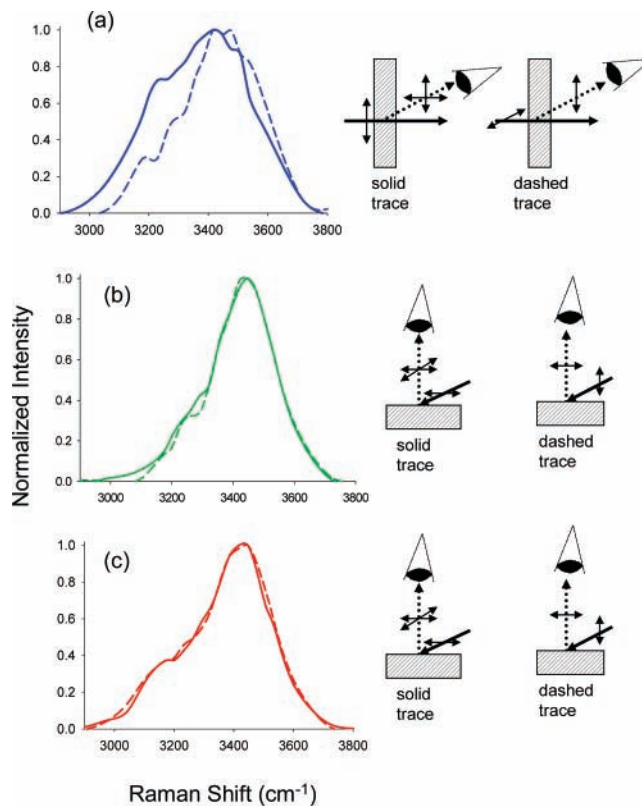

Figure 1. Raman spectra of the OH-stretching region of (a) room-temperature bulk water, (b) the air−water interface, and (c) the air−ice interface at −15 °C. Solid traces correspond to vertical polarization in the bulk and s-polarized radiation at the surface, and dashed traces correspond to horizontally polarized light in the bulk and p-polarized light at the surface. The insets illustrate the experimental geometry used in each case. Here the solid line shows the input laser and the dotted line shows the scattered light.

solution of the desired compound into a Pasteur pipet and then expelling the collected gas onto the ice surface.

Dodecane samples were prepared by spreading a small amount (∼0.1 mL) of dodecane on a glass microscope slide and placing it in the reaction chamber. The chamber was purged for 10 min with dry nitrogen prior to inserting the dodecane sample in the chamber, as well as during data acquisition.

3. Chemicals. Acridine (Fluka, ≥97.0%), dodecane (Sigma Aldrich, ≥99%), concentrated nitric acid (Caledon, ≥99.9%), reagent grade concentrated hydrochloric acid (Baker) and ammonium hydroxide (Fisher), and nitrogen gas (BOC, >99.99%) were used as purchased. Ice was prepared from 18 MΩ deionized water for all Raman experiments and from distilled water for all LIF experiments.

Results

1. General features of Raman Spectra at Water and Ice Surfaces. The Raman spectrum of the OH-stretch region of water has been well studied (e.g., ref 14 and references therein). Figure 1a shows intensity-normalized spectra of bulk water measured using vertically (solid trace) and horizontally (dashed trace) polarized input radiation. In our experimental geometry, the scattered light in the former case contains components with polarization both parallel and perpendicular to that of the input light; the latter contains only the perpendicular polarization component in the scattered signal arising from depolarization. Hence the spectrum shown by the solid trace contains contributions that transform as both symmetric and antisymmetric stretching vibrations in liquid water.[14] The dashed trace arises

only from the depolarized scattering from vibrations which transform as antisymmetric stretches. Although we do not separate the parallel and perpendicular components of the scattered light, the solid trace shown in Figure 1a is essentially identical to the unpolarized spectrum reported by others, in which the parallel component of the scattered light contributes the greatest part to the observed signal.[14] We shall therefore hereafter refer to this component as the "unpolarized spectrum".

Whereas in the isolated water molecule the symmetric stretch vibration lies at a lower energy than the antisymmetric stretch, in the liquid state both of these vibrations are red-shifted with respect to the antisymmetric stretch of the isolated molecule, due to the extensive hydrogen-bonded nature of the liquid. The large shoulder on the low-wavenumber side ($\sim$3200 cm^{-1}) of the solid trace in Figure 1a is assigned[15] to vibrations involving more highly hydrogen bonded ("4-coordinate") molecules, by analogy with the spectrum of bulk ice, in which this feature dominates.[15] The higher frequency band has been assigned (for spectra corresponding to that shown in the solid trace) to vibrations involving less strongly hydrogen-bonded molecules.[15] Because this high-frequency component transforms as an asymmetric vibration, it appears in the dashed-line spectrum. A recent reinterpretation of vibrational water spectra by Petersen and Saykally[16] posits that there exists a continuum of hydrogen bonding states in the bulk liquid and that the appearance of two bands in the parallel spectrum should not be associated with two distinct hydrogen-bonding environments. Consequently, in the following we shall discuss the results as indicating "more" or "less" hydrogen-bonded environments, with no further quantification.

Parts b and c of Figure 1 show intensity-normalized spectra of the OH-stretching band of water taken with the laser impinging on a water surface (Figure 1b) and on an ice surface (Figure 1c), at an incident angle >87° from the surface normal. Here the detection is above the plane of the interface; therefore, p-polarized input radiation (vertical polarization) allows detection of the perpendicularly polarized (i.e., depolarized) spectrum and s-polarized input light (horizontal polarization) allows detection of both the parallel and perpendicularly polarized scattered light. The solid and dashed lines in these figures represent the spectra measured using s- and p-polarized input radiation, respectively, and can thus be compared directly to the corresponding solid and dashed line traces shown in Figure 1a. The spectra illustrated by the solid lines are clearly much narrower for surface scattering than for bulk scattering, primarily due to a significant loss of intensity from the low-energy side of the band. The depolarized scattering spectra, shown by the dashed lines, are quite similar in overall shape to the spectra observed using s-polarized radiation for both the liquid and solid water surfaces. It is interesting to note that the strong polarization dependence observed for bulk water is observed only very faintly for the air−water interface and is not seen at all at the air−ice interface.

In Figure 2 the "unpolarized" spectra observed from the water bulk, water surface, ice surface, and solid ice bulk, are plotted together for comparison. In the near-surface region, the local environment is expected to contain fewer highly coordinated water molecules; consequently, if there is a significant contribution to the Raman spectrum from this region, a less intense red shoulder to the band is expected. Indeed the s-polarized water spectrum in Figure 2 shows significantly less intensity at low energies than does the unpolarized bulk water spectrum. As well, the ice surface spectrum is significantly blue-shifted compared to the bulk ice spectrum; both ice and supercooled water are
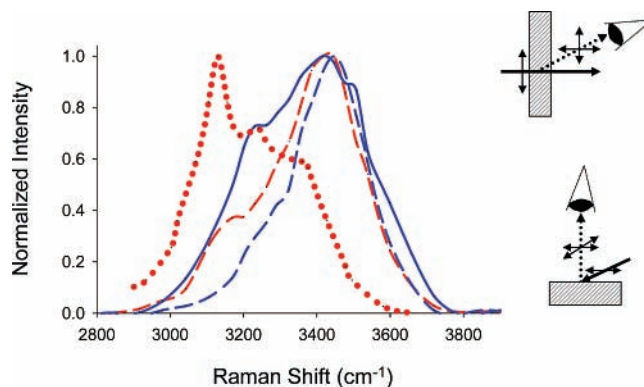

Figure 2. Intensity-normalized unpolarized Raman spectra of the OH-stretching region of room-temperature bulk water (solid blue trace), the air−water interface (dashed blue trace), bulk ice at −20 °C (dotted red trace), and the air−ice interface at −15 °C (dashed red trace). The bulk ice spectrum has been redrawn on the basis of Figure 4 of ref 39.
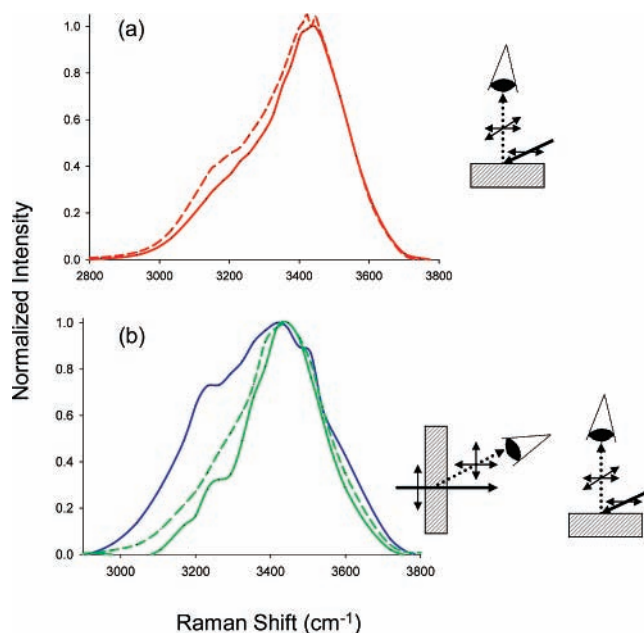

Figure 3. Intensity-normalized Raman spectra: (a) the OH-stretching region of the air−ice interface at −0.5 °C (solid trace) and −13.5 °C (dashed trace); (b) the OH-stretching region of room-temperature bulk water (blue solid trace) and the air−water interface with an incident laser angle 87.2° from the surface normal (green solid trace) and 40° from the surface normal (green dashed trace). Experimental geometries are as illustrated in the insets.

dominated[17] by a feature near 3200 cm^{-1}, with a shoulder at higher energy which corresponds to the dominant feature in the room-temperature liquid. These spectra suggest that the liquid water surface displays the least amount of water−water hydrogen bonding, followed by the ice surface and then by bulk water and finally bulk ice. Figure 3a displays spectra of the ice surface measured using s-polarized light at temperatures near 0 and −15 °C. A clear increase in the relative intensity of the red shoulder is observed as the temperature is lowered, consistent with this interpretation.

To test this further, we measured the Raman spectrum from the water surface at a laser incidence angle of 40° from the surface normal. At this angle 0.6% of p- and 4.3% of s-polarized light is reflected, as compared to 65.5% and 78.8%, respectively at 87° from the surface normal. The result, shown in Figure 3b, clearly shows a broadening to the red side of the spectrum at the less glancing angle, consistent with a greater contribution from the bulk in this case.
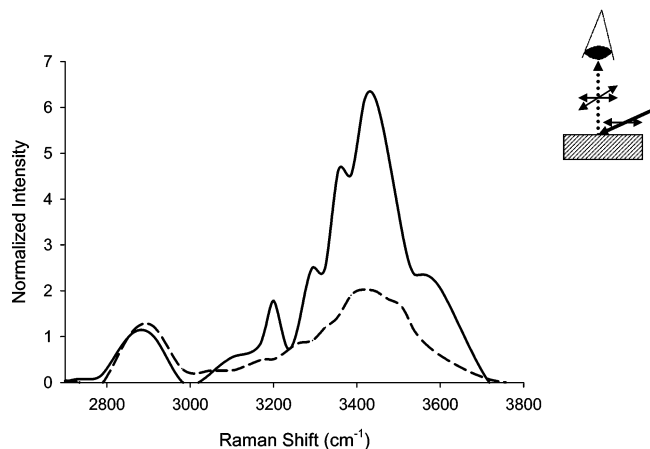
Probes of the Quasi-Liquid Layer on Ice

J. Phys. Chem. A, Vol. 111, No. 43, 2007 **11009**

Figure 4. Raman spectra of a room temperature dodecane surface under a flow of dry nitrogen with incident laser angles 87.2° from the surface normal (solid trace) and 80° from the surface normal (dashed trace). The spectra are normalized to the CH-stretch fraction at ~2900 cm^{-1}. Experimental geometries are as illustrated in the inset.

Figure 5. Ratio of the intensity at 2395 cm^{-1} to that at 3450 cm^{-1} on D$_2$O ice at -15 °C under a flow of dry nitrogen (blue squares) and under a flow of water vapor in nitrogen (red triangles).

Sum frequency generation (SFG) measurements of the ice surface[8] have observed an effect of changing the temperature similar to that shown in Figure 3. The orientation of hydroxyl groups in the surface layer of the QLL becomes more disordered as temperatures increase from 200 K to the melting point. Clear differences in the amount of disorder of the surfacial water molecules are observed at the surfaces of ice and of supercooled water at identical temperatures,[8] suggesting that the surface region of the air–ice interface is structurally different from water surfaces, supercooled or otherwise.

2. Surface Sensitivity of the Raman Probe. The differences observed in the OH-stretch region between bulk and surface water and between bulk and surface ice suggest that we are seeing different environments at the surface and in the bulk. This interpretation assumes that there is sufficient intensity associated with the scattering generated in the surface region to be distinguished from the bulk contribution. In the following section we will discuss the results of experiments that were designed to explore our sensitivity to the ice and water surfaces.

(a) Observing Water on Dodecane Surfaces. In this experiment, we measured the water OH-stretch spectrum at the surface of liquid dodecane. Water is not miscible with dodecane but will adsorb (or condense) onto its surface in amounts which depend on the ambient relative humidity. The uptake of water by this compound has been determined as a function of relative humidity in this laboratory.[18] At a room-temperature relative humidity approaching 100%, a maximum of ~50 monolayers of water are present at the dodecane surface. Figure 4 shows two s-polarized Raman spectra measured at a dodecane surface under low relative humidity conditions, with incidence angles for the excitation laser beam of 80° from the surface normal (dashed trace) and 87° from the normal (solid trace). The intensity at 2900 cm^{-1} arises from the dodecane CH-stretch, but the water OH-stretch, appearing at ~3450 cm^{-1}, is clearly observed in both spectra. This result clearly shows that this technique is sensitive to a surfacial water layer of ~50 monolayers, or a probe depth of ~15 nm. It should be noted that this is a conservative estimate, as the cited 50 monolayers of water is only present under extremely high relative humidity, which was not the case in our measurements. Further, we have also measured water OH-stretch bands on glass surfaces at ambient relative humidity, which likely corresponds to fewer than five molecular layers of water.[19]
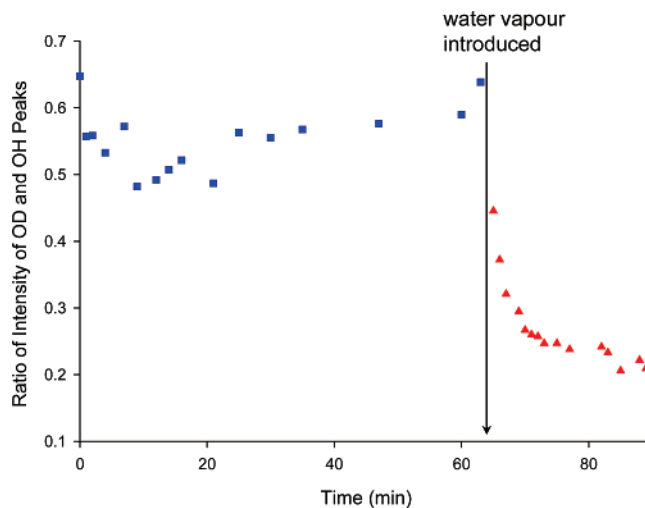
The angle dependence of the spectra shown in Figure 4 is also consistent with the notion that we are sensitive to the dodecane surface region: The relative intensity of the water OH-stretch increases as the laser angle becomes more glancing. This effect, similar to that illustrated in Figure 3a, is consistent with the expectation that at a more glancing incidence angle, more light is reflected from the sample surface, resulting in the observed spectrum containing a smaller contribution from the underlying bulk sample (dodecane in this instance).

(b) Water Condensation on D$_2$O Ice. In a second experiment we measured the ice surface spectrum while flowing H$_2$O vapor over D$_2$O ice. Since the Raman OD-stretch appears at lower energies than the OH-stretch (on ice, we observe peak intensities at 2395 and 3450 cm^{-1}, respectively), we can readily monitor the ratio of the intensities of these two peaks as a function of time. A decrease in the OD/OH intensity ratio is expected, due to the condensation of H$_2$O on the D$_2$O ice surface.

Figure 5 shows the time dependence of the intensity ratio of these two peaks as H$_2$O vapor flows over a D$_2$O ice sample. In our experimental setup, it was not possible to eliminate a contribution from the OH-stretch to the D$_2$O ice spectra due to condensation of ambient water vapor onto the ice. (Measurements of the bulk liquid spectrum of D$_2$O contained a negligible contribution from OH, however.) Nevertheless, in Figure 5 one sees that the OD/OH ratio remains fairly constant over a large time period while dry nitrogen flows across the D$_2$O ice sample, but when H$_2$O vapor is introduced to the nitrogen stream, an immediate and rapid decrease in the OD/OH ratio is observed. The intensity ratio levels off within a few minutes and remains constant thereafter. A reduction in the OD/OH intensity ratio is also seen when ~1 cm^3 of air containing ~6 × 10^{17} molecules of H$_2$O(g) is introduced via a Pasteur pipet. In this instance the decrease is ~15–20% of that observed in Figure 5. Assuming the gas introduced to the ice surface is saturated with H$_2$O vapor and that every water molecule present in the pipet collides with the ice surface, we estimate deposition of between 20 and 200 molecular layers, for an accommodation coefficient in the range 0.1–1.

Isotopic switching at the D$_2$O ice surface is expected to rapidly convert both the original D$_2$O and the adsorbing H$_2$O to HOD. Subsequent diffusion of HOD through ice films is believed to be negligible.[20] Therefore, we interpret the observed decrease in the OD/OH signal as being due to condensation and isotopic scrambling of H$_2$O at the ice surface. This
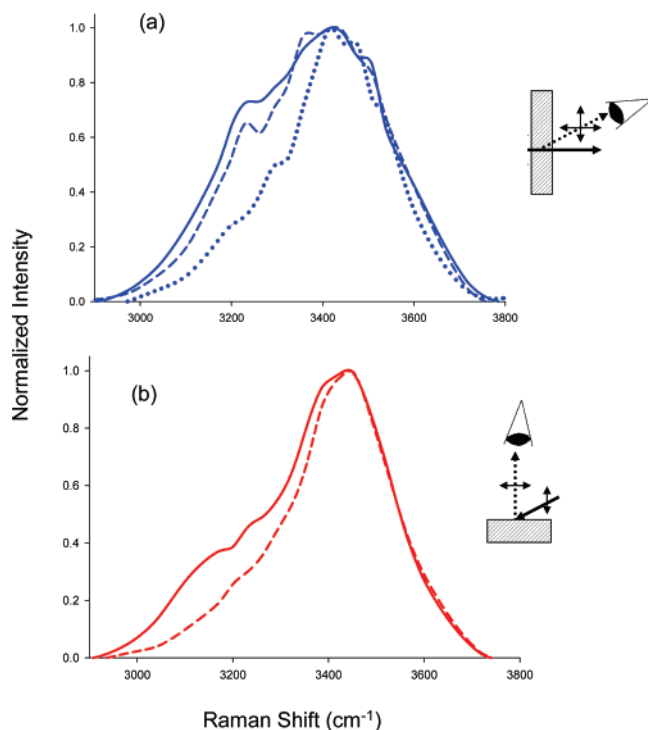
Figure 6. Intensity-normalized Raman spectra of the OH-stretching region of (a) room-temperature bulk water (solid trace), a 1 mol L^{-1} NaCl solution (dashed trace), and a 4 mol L^{-1} NaCl solution (dotted trace) and (b) the surfaces of pure ice at -15 °C (solid trace) and a frozen 0.01 mol L^{-1} NaCl solution at the same temperature (dashed trace). Experimental geometries are as illustrated in the insets.

observation, and that discussed in the previous section, give us confidence that the glancing-angle Raman probe is sensitive to changes in the surface region of ice over a (conservative) range of tens to hundreds of monolayers.

3. Effects of Contaminants on the Spectra. In section 2 we argued that the glancing-angle Raman technique may be used to infer aspects of the water ice surface environment. In the following, we show how Raman spectra measured at the ice surface are sensitive to changes in the local environment which may be induced by different solutes.

Atmospheric and terrestrial ice is rarely pristine. Gaseous acids, such as HCl and HNO$_3$, adsorb readily to ice, both on the Earth and in high-altitude cirrus clouds (e.g., refs 21 and 22). Sea salt is ubiquitous on sea ice,[23,24] and halogen chemistry initiated by oxidation of ice-bound halides is extremely important to ozone loss in the polar boundary layer (see for example ref 25 and references therein). In addition to being involved directly in ozone destruction, sea salt present on ice could affect the structure of the QLL and thus its physical and chemical interactions with pollutants. In urban centers a wide variety of contaminants, potentially including road salt, could be present in high concentrations.

Figure 6a shows the effect of dissolved NaCl on the OH-stretch region of the bulk water Raman spectrum. The low wavenumber region in pure water (solid trace) is diminished in intensity in a 1 mol L^{-1} solution of NaCl, as displayed by the dashed trace. Increasing the NaCl concentration to 4 mol L^{-1} (dotted trace) diminishes the intensity in this region even further. Sodium halide salts disrupt the hydrogen-bond network of bulk water, which leads to the observed reduction in Raman intensity at low energies of the OH-stretch region.[15] At the air−water interface, a shift in the spectrum toward higher energies has been observed by SFG studies in the presence of NaBr and NaI,
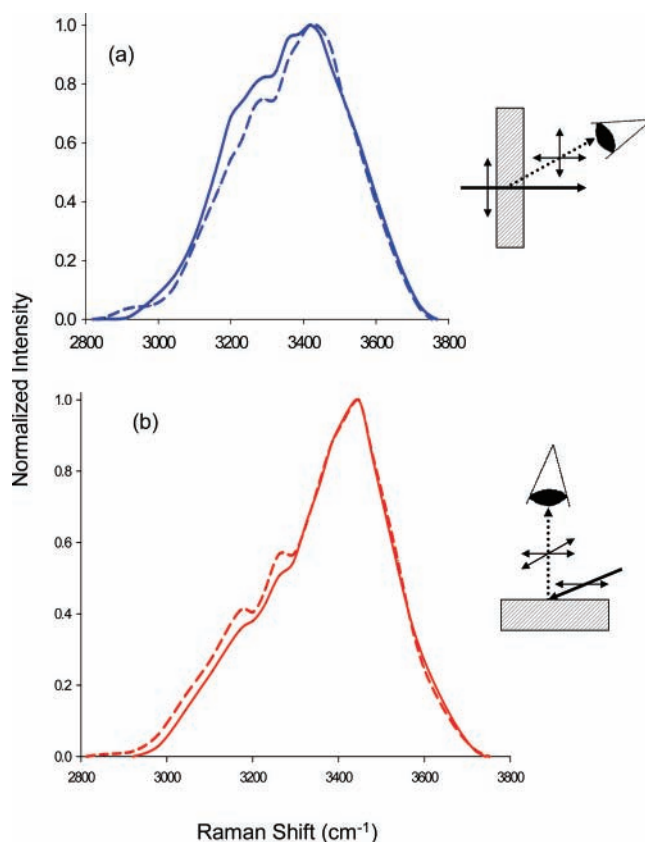

Figure 7. Intensity-normalized Raman spectra of the OH-stretching region (a) of room-temperature bulk water (solid trace) and of a 1 mol L^{-1} HCl solution (dashed trace) and (b) of a pure ice surface at -15 °C (solid trace) and of the same ice surface after the deposition of gaseous HCl (dashed trace). Experimental geometries are as illustrated in the insets.

although NaCl does not change the spectrum.[26] We do not see any effect on the s-polarized spectrum at the water surface in the presence of up to 4 mol L^{-1} NaCl, but on ice we see a reduction in intensity in the red portion of the spectrum when dilute NaCl solutions are frozen at -15 °C. Figure 6b illustrates this for solutions with initial NaCl concentrations of 0.01 mol L^{-1}. The decrease in the area under the intensity-normalized curves relative to the pure ice spectrum is ∼14%, with the loss occurring almost entirely from the red end of the spectrum. The effect of NaCl on the ice surface spectrum is much greater than that observed for bulk water, where a decrease in the area under the curve of ∼10% is not observed for NaCl concentrations below 1 mol L^{-1}.

Exclusion of NaCl during freezing is a well-known phenomenon, and at the temperatures used in this experiment (ca. -15 °C), this process is expected to result in a combination of pure ice and concentrated NaCl solution (∼10 mol L^{-1}) at the ice surface or in the QLL. Our observations of reduced intensity at 3200 cm^{-1}, illustrated in Figure 6, could therefore be interpreted either as disruption of hydrogen bonding in the QLL or as the formation of a liquid-phase brine at the ice surface; the corresponding spectra resemble those obtained at the air−water interface. We are unable to distinguish between the two phenomena using this technique, as a disruption in hydrogen bonding of the QLL will inevitably shift the Raman spectrum toward that of the less-strongly H-bonded liquid water surface.

The effect of the presence of 1 mol L^{-1} HCl on the Raman OH-stretch band of bulk water, shown in Figure 7a, indicates that HCl disrupts hydrogen bonding in the bulk to the same extent as NaCl. Surface Raman spectra of concentrated HCl
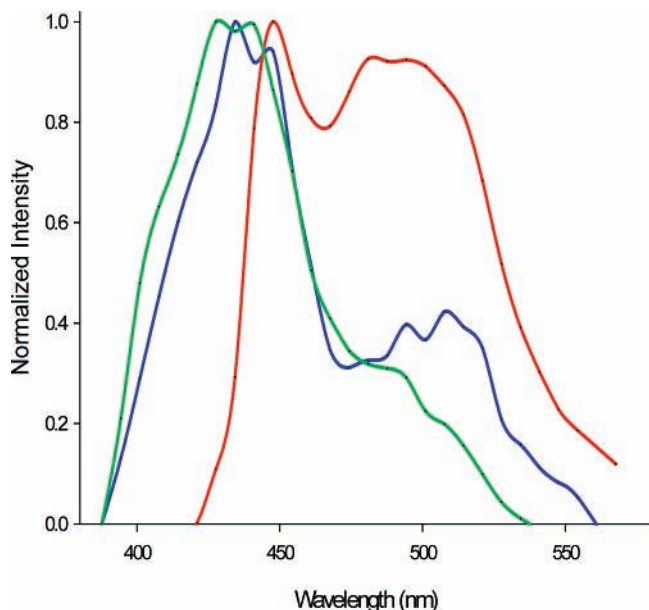
Probes of the Quasi-Liquid Layer on Ice

J. Phys. Chem. A, Vol. 111, No. 43, 2007 **11011**

Figure 8. Acridine fluorescence spectra at a pure ice surface at −15 °C (blue trace), after deposition of gaseous HNO$_3$ (red trace), and at the surface of the melted acidic sample (green trace).

solutions at room temperature are indistinguishable from those of pure water. However, by contrast, Figure 7b shows that depositing gas-phase HCl onto an ice surface results in *increased* intensity at low energies. This small increase (of ∼3%) is also observed upon exposure of the ice to HNO$_3$(g), while NH$_3$(g) deposited on the ice surface decreases the intensity at low energies by a similar magnitude.

To help explain these observations, we turn to another surface-sensitive spectroscopic probe. Acridine is a surface-active heteroatom-containing PAH with a pKa of ∼5.5. Its wavelength-resolved fluorescence spectrum is a convolution of emission from its neutral and protonated forms, which have peak fluorescence intensities at ca. 430 and 480 nm, respectively. The ratio of the fluorescence intensities at these wavelengths can be used to determine the pH of a solution; this technique has been used to probe the pH of aqueous droplets[27] and has been used in this laboratory to probe pH changes at the air–aqueous interface.[28]

Here, we adapt this method to probe the ice surface. The experimental setup is identical with that used for our Raman studies, except that the Nd:YAG laser was exchanged for a nitrogen laser emitting at 337 nm and ice samples were prepared from distilled water rather than deionized water to have a higher initial pH.

Figure 8 shows acridine fluorescence spectra acquired at the air–ice interface before and after introducing a maximum of 8 × 10^{16} molecules gas-phase HNO$_3$ to the surface of a frozen acridine solution. In the present experimental arrangement, we cannot quantify the number of gas phase acid molecules which adsorb to the ice surface, as an unknown fraction of the input vapor will be taken up by all the other surfaces present. Upon addition of the acid, the fluorescence spectrum of acridine, shown as the blue trace, undergoes a significant red shift, as illustrated by the red trace, indicating a significant drop in the pH at the ice surface. When the sample is melted, the acridine spectrum shifts back to that of the neutral species, displayed as the green trace in the figure, as the nitric acid dissolves into the bulk sample. Acridine fluorescence also shows a similar decrease in the local pH when either HCl or acetic acid is used

as a trace probe gas. This spectral shift can be reversed by puffing ammonia onto the acid-doped ice surface.

It is unlikely that surface melting of the ice due to the high partial pressures of acids used in our experiments is occurring. The reduced intensity at 3200 cm^{-1} in the Raman spectra of frozen NaCl solutions could be due to the formation of a surficial brine, as discussed above. By contrast, the observed increase in relative intensity at 3200 cm^{-1}, shown in Figure 7b when HCl(g) and HNO$_3$(g) are introduced to the ice surface, is inconsistent with the idea that surface melting gives rise to a decrease in hydrogen bonding under these conditions.

In order for changes in pH to occur, the gas phase acid must dissociate. The result displayed in Figure 8 is important, as it indicates that, over the course of an experiment, the adsorbed acids do dissociate to ions and remain in the surface region. Flowtube studies performed with atmospherically relevant partial pressures of nitric acid and HCl indicate that the majority of the acid is irreversibly adsorbed to ice surfaces, presumably due to ionization of the acid on the surface.[29,30] Coupled uptake–elipsometry experiments suggest that HCl uptake can induce structural disorder at the ice surface, interpreted as being due to formation of a QLL.[31] Transmission FTIR spectroscopy indicates that nitric acid dissociates on ice surfaces at temperatures below 150 K,[32] and our results show that dissociation/ionization of these acids takes place at ice surfaces at temperatures warmer than −16 °C.

The dissociation of HCl and HNO$_3$ in the QLL will lead to the formation of hydronium ions, which may be strongly hydrogen bonded to at least three other water molecules and which are believed to show some propensity for the surface of aqueous solutions.[33] This is a likely explanation for the enhancements in Raman intensity observed at low energies in the presence of HCl and HNO$_3$. Likewise, decreased Raman intensity in the presence of NH$_3$ can be explained by this molecule's propensity to scavenge protons. The resulting NH$_4^+$ is evidently similar to Na$^+$ in its effects on the hydrogen-bonding structure at the ice surface.

Atmospheric Implications

Understanding the physical properties of the QLL is important to atmospheric scientists primarily for its potential effects on chemical reactivity. Many important atmospheric reactions occur on ice surfaces, but their mechanisms and kinetics are by and large not well understood. It is convenient to treat the QLL as a thin film of liquid water in which all reactions on ice surfaces occur, as this allows aqueous phase kinetics to be extrapolated to subfreezing temperatures. However, the validity of this treatment has been questioned,[34] and results from this laboratory confirm that this is not always appropriate. Raman spectra acquired in this study show that hydrogen bonding at the air–ice interface occurs to a different extent than in bulk water or at the air–water interface. We also show that the effects of solutes such as NaCl and HCl on hydrogen bonding can be dramatically different at the air–ice interface and in bulk water. Recent studies have shown significant differences in the direct[12,13] and indirect[12,35] photolysis rates of PAHs at the air–ice interface compared to at the air–water interface or in bulk water. These results indicate that the QLL presents a very different environment from that of liquid water and that the reactivity of a compound on ice could be very different from that in liquid water or at the air–water interface.

Our glancing-angle LIF probe provides a straightforward method of monitoring pH changes at the air–ice interface. The reactivities of a number of environmentally relevant compounds

are pH-dependent, but determining the pH of the QLL has proved to be very challenging due to its extremely small volume. This is often dealt with by calculating the pH of the QLL by assuming that all solutes are expelled into the QLL during freezing (for example, see refs 36 and 37). Once again, the validity of this assumption has not been confirmed.[34] Used incorrectly, the assumption of full exclusion could lead to errors in [H$^+$] of several orders of magnitude. While our LIF technique is not configured to measure absolute pH values, its ability to monitor changes in the pH of the QLL can aid in understanding the effects of solutes on pH. Indeed, upon refreezing of the solution shown as the green trace in Figure 8, the acridine fluorescence spectrum did not shift to that of the protonated species, which might indicate that the dissolved nitric acid was not excluded to the ice surface.

Finally, it is worth asking what we can learn by measuring various properties of the QLL. In terms of atmospheric chemistry, the ultimate goal is generally to understand the QLL in terms of a chemical solvent or substrate. Knowing whether the air–ice interface should be treated as a thin film of liquid water, as a solid substrate, or whether some other description must be used would make heterogeneous processes that occur on ice surfaces amenable to quantitative modeling. However, as discussed in the Introduction, different probes measure very different values for properties of the QLL, such as density and depth as functions of temperature. It is likely that that these properties are not homogeneous throughout the QLL and that there may be no "true" value that can be ascribed to them.

In this case, it might be worthwhile to focus on the effects the QLL has on solutes present at the air–ice interface. Results from this study and from a previous study[12] highlight some of the information that can be gained from such investigations. Extensive self-association of the PAHs naphthalene and anthracene on ice surfaces indicates that solvation of these compounds occurs much less readily at the air–ice interface than at the air–water interface. This observation, combined with very different direct and indirect PAH photolysis kinetics observed at solid and liquid aqueous surfaces, suggests that the QLL presents a very different environment to PAHs than does a liquid water surface.[12] Conversely, changes in the emission spectrum of acridine upon the introduction of gas-phase acids and bases to the ice surface suggest that the dissociation of these species occurs as readily in the QLL as at an air–water interface. This shows that different solutes may be affected differently by the QLL and that the behavior of one compound cannot necessarily be predicted on the basis of that of other species.

Conclusions

We have developed a novel tool for monitoring the structure of the QLL under different physical conditions. This glancing-angle Raman spectroscopy probe is sensitive to changes taking place within the upper ~50 monolayers of water and is thus capable of detecting changes occurring at the air–ice interface. A complementary technique using glancing-angle LIF of acridine enables us to see changes in pH at the ice surface. Using these two techniques, we have inferred the ionization of gaseous acids and bases deposited onto ice surfaces and have related this to structural changes observed in the QLL. The presence of acids appears to enhance hydrogen bonding in the QLL, likely due to enhanced H$_3$O$^+$ concentrations. These observed structural changes are inconsistent with surface melting leading to greater contribution to the signal from bulk water. Our observations are largely consistent with SFG measurements at the surfaces of ice[8] and aqueous salt and acid solutions.[15,26,38]

References and Notes

(1) Beaglehole, D.; Nason, D. *Surf. Sci.* **1980**, *96*, 357.

(2) Doppenschmidt, A.; Butt, H.-J. *Langmuir* **2000**, *16*, 6709.

(3) Elbaum, M.; Lipson, S. G.; Dash, J. G. *J. Cryst. Growth* **1993**, *129*, 491.

(4) Engemann, S.; Reichert, H.; Dosch, H.; Bilgram, J.; Honkimaki, V.; Snigirev, A. *Phys. Rev. Lett.* **2004**, *92*, 205701.

(5) Golecki, I.; Jaccard, C. *Phys. Lett.* **1977**, *63A*, 374.

(6) Lied, A.; Dosch, H.; Bilgram, J. H. *Phys. Rev. Lett.* **1994**, *72*, 3554.

(7) Sadtchenko, V.; Ewing, G. E. *J. Chem. Phys.* **2002**, *116*, 4686.

(8) Wei, X.; Miranda, P. B.; Shen, Y. R. *Phys. Rev. Lett.* **2001**, *86*, 1554.

(9) Rosenberg, R. *Phys. Today* **2005**, *58*, 50.

(10) Pincock, R. E. *Acc. Chem. Res.* **1969**, *2*, 97.

(11) Takenaka, N.; Ueda, A.; Daimon, T.; Bandow, H.; Dohmaru, T.; Maeda, Y. *J. Phys. Chem.* **1996**, *100*, 13874.

(12) Kahan, T. F.; Donaldson, D. J. *J. Phys. Chem. A* **2007**, *111*, 1277.

(13) Dubowski, Y.; Hoffmann, M. R. *Geophys. Res. Lett.* **2000**, *27*, 3321.

(14) Reid, J. P.; Meresman, H.; Mitchem, L.; Symes, R. *Int. Rev. Phys. Chem.* **2007**, *26*, 139.

(15) Gopalakrishnan, S.; Liu, D.; Allen, H. C.; Kuo, M.; Shultz, M. J. *Chem. Rev.* **2006**, *106*, 1155.

(16) Petersen, P. B.; Saykally, R. J. *Annu. Rev. Phys. Chem.* **2006**, *57*, 333.

(17) Hare, D. E.; Sorensen, C. M. *J. Chem. Phys.* **1992**, *96*, 13.

(18) Demou, E.; Visram, H.; Donaldson, D. J.; Makar, P. A. *Atmos. Environ.* **2003**, *37*, 3529.

(19) Sumner, A. L.; Menke, E. J.; Dubowski, Y.; Newberg, J. T.; Penner, R. M.; Hemminger, J. C.; Wingen, L. M.; Brauers, T.; Finlayson-Pitts, B. J. *Phys. Chem. Chem. Phys.* **2004**, *6*, 604.

(20) Oxley, S. P.; Zahn, C. M.; Pursell, C. J. *J. Phys. Chem. A* **2006**, *110*, 11064.

(21) MacTaylor, R. S.; Gilligan, J. J.; Moody, D. J.; Castleman, A. W., Jr. *J. Phys. Chem.* A **1999**, *103*, 4196.

(22) Voigt, C.; Schlager, H.; Ziereis, H.; Karcher, B.; Luo, B. P.; Schiller, C.; Kramer, M.; Popp, P. J.; Irie, H.; Kondo, Y. *Geophys. Res. Lett.* **2006**, *33*, LO5803.

(23) Domine, F.; Sparapani, R.; Ianniello, A.; Beine, H. J. *Atmos. Chem. Phys.* **2004**, *4*, 2259.

(24) Massom, R. A.; Eicken, H.; Haas, C.; Jeffries, M. O.; Drinkwater, M. R.; Sturm, M.; Worby, A. P.; Wu, X.; Lytle, V. I.; Ushio, S.; Morris, K.; Reid, P. A.; Warren, S. G.; Allison, I. *Rev. Geophys.* **2001**, *39*, 413.

(25) Simpson, W. R.; von Glasow, R.; Riedel, K.; Anderson, P.; Ariya, P.; Bottenheim, J.; Burrows, J.; Carpenter, L.; Friess, U.; Goodsite, M. E.; Heard, D.; Hutterli, M.; Jacobi, H.-W.; Kaleschke, L.; Neff, B.; Plane, J.; Platt, U.; Richter, A.; Roscoe, H.; Sander, R.; Shepson, P.; Sodeau, J.; Steffen, A.; Wagner, T.; Wolff, E. *Atmos. Chem. Phys. Discuss.* **2007**, *7*, 4285.

(26) Liu, D.; Ma, G.; Levering, L. M.; Allen, H. C. *J. Phys. Chem. B* **2004**, *108*, 2252.

(27) Sayer, R. M.; Gatherer, R. D. B.; Reid, J. P. *Phys. Chem. Chem. Phys.* **2003**, *5*, 3740.

(28) Clifford, D.; Bartels-Rausch, T.; Donaldson, D. J. *Phys. Chem. Chem. Phys.* **2007**, *9*, 1362.

(29) Abbatt, J. P. D. *Geophys. Res. Lett.* **1997**, *24*, 1479.

(30) Cox, R. A.; Fernandez, M. A.; Symington, A.; Ullerstam, M.; Abbatt, J. P. D. *Phys. Chem. Chem. Phys.* **2005**, *7*, 3434.

(31) McNeill, V. F.; Loerting, T.; Geiger, F. M.; Trout, B. L.; Molina, M. J. *Proc. Natl. Acad. Sci. U.S.A.* **2006**, *103*, 9422.

(32) Pursell, C. J.; Everest, M. A.; Falgout, M. E.; Sanchez, D. D. *J. Phys. Chem. A* **2002**, *106*, 7764.

(33) Jungwirth, P.; Tobias, D. J. *Chem. Rev.* **2006**, *106*, 1259.

(34) Domine, F.; Albert, M.; Huthwelker, T.; Jacobi, H.-W.; Kokhanovsky, A. A.; Lehning, M.; Picard, G.; Simpson, W. R. *Atmos. Chem. Phys. Discuss.* **2007**, *7*, 5941.

(35) Klanova, J.; Klan, P.; Heger, D.; Holoubek, I. *Photochem. Photobiol. Sci.* **2003**, *2*, 1023.

(36) Chu, L.; Anastasio, C. *J. Phys. Chem.* **2003**, *107*, 9594.

(37) Chu, L.; Anastasio, C. *J. Phys. Chem. A* **2005**, *109*, 6264.

(38) Levering, L. M.; Sierra-Hernandez, M. R.; Allen, H. C. *J. Phys. Chem. C* **2007**, *111*, 8814.

(39) Fukazawa, H.; Mae, S.; Ikeda, S. *Ann. Glaciol.* **2000**, *31*, 247.